COMPENSATION OF COARSENESS ERROR IN TLM MODELING OF MICROWAVE STRUCTURES WITH THE SYMMETRICAL CONDENSED NODE

J. L. Herring and W. J. R. Hoefer

NSERC/MPR Teltech Research Chair in RF Engineering, Department of Electrical & Computer Engineering, University of Victoria, P.O. Box 3055 M.S. 8610, Victoria, B.C., Canada, V8W 3P6.

ABSTRACT

The coarseness error inherent in a TLM simulation involving sharp edges is reduced by increasing the speed of pulse propagation around the discontinuity with only a local mesh modification. The implementation of the technique is described in detail and the method is applied to a narrow band E-plane filter.

INTRODUCTION

The transmission-line matrix (TLM) method of numerical electromagnetic analysis in three dimensions with the symmetrical condensed node (SCN) [1] is well established. However, if edges or corners are present then it is often found that frequency domain characteristics are shifted towards lower frequencies. This can be overcome by increasing the mesh resolution, but finite computer resources impose limits on this approach. It is possible to get improved results by reducing the timestep only (keeping the spatial resolution constant), provided that a node with good dispersion characteristics is selected. This may require only a small increase in storage but the run-time problem remains. Graded mesh [2] or multiple grid [3] techniques can be used, but the resources are still greater than for a simple coarse mesh in which the resolution is determined solely by the highest frequency of interest.

A technique is required in which a local modification is made around the discontinuity, imposing only a small computational burden. Previously, inductive stubs have been added to two dimensional TLM nodes with good results [4]. A general three dimensional technique has been applied to the modeling of wires, in which the velocity of the pulses in the vicinity of the discontinuity is increased at the expense of a reduction in timestep for the whole problem space [5]. In this paper, a method which does not require a global change in timestep [6] is described in detail.

THE NEW METHOD

To apply the method to the structure shown in Fig. 1, a modification is made to the four nodes surrounding the end of the septum, which is modeled with a short-circuit boundary placed between nodes. The time taken for voltage pulses to travel around the end of the septum is reduced by eliminating the delay associated with the link-lines. The set of four nodes can be treated as a "supernode" in which the internal link-lines are not present. Alternatively, the internal pulses can be calculated first and then the standard scattering procedure can be applied to the four nodes separately. This second method can be implemented more simply and this is the approach adopted here. No special treatment is required for pulses travelling parallel to the septum.

In the absence of stubs, the internal pulses can be calculated using the standard scattering matrix, provided that this is done in the order shown in Fig. 2a. However, stubs are required to increase the capacitance and inductance so that the correct result is obtained. In this case, the internal voltage pulses are mutually dependant and it is necessary to solve for all internal pulses simultaneously. This is done by equating the incident and reflected pulses from adjacent nodes and solving the resulting simultaneous equations to yield expressions for the internal pulses in terms of the external pulses only. These expressions can then be simplified to reduce the number of arithmetic operations which must be performed.

IMPLEMENTATION

For the SCN in which open-circuit stubs (coupling with the electric field) are used to model increased capacitance and short-circuit stubs (coupling with the magnetic field) are used to model increased inductance, a computationally efficient way of writing the scattered pulses is [7]:

$$V^r_{inj} = V_j + Z_0 \cdot I_k - V^i_{ipj} \qquad V^r_{ipj} = V_j - Z_0 \cdot I_k - V^i_{inj}$$

where i, j and k subscripts are the directions (x, y or z), Z_0 is the link-line characteristic impedance and the three voltage pulse subscripts denote the direction of the link-line, 'n' or

'p' for the negative or positive side of the node (taking the origin at the centre), and the link-line polarization. The node voltages and loop currents are given by:

$$V_i = k_{ei}(V^i_{jni} + V^i_{jpi} + V^i_{kni} + V^i_{kpi} + \hat{Y}^s_i \cdot V^i_{ei})$$
$$I_i = k_{mi}(V^i_{jpk} - V^i_{jnk} - V^i_{kpj} + V^i_{knj} - V^i_{mi})$$

where

$$k_{ei} = 2/(4 + \hat{Y}^s_i) \qquad \text{and} \qquad k_{mi} = 2/Z_0(4 + \hat{Z}^s_i)$$

V^i_{ei} and V^i_{mi} are the voltage pulses incident from the stubs coupling with the electric and magnetic fields, respectively, and $\hat{Y}^s_i$ and $\hat{Z}^s_i$ are the corresponding normalized stub admittances and impedances. For maximum flexibility, the stubs can be different in each direction, in the same way as for anisotropic materials with diagonal permittivity and permeability tensors. This is a simple extension from the isotropic case.

For the four nodes shown in Fig. 2b, it is best to first calculate the internal pulses between nodes C and D. For the y polarization:

$${}_C V^i_{xpy} = ({}_{AC}a_y \cdot {}_{BD}\zeta_y - {}_{BD}b_y \cdot {}_{AC}\zeta_y)/c_y$$
$${}_D V^i_{xny} = ({}_{BD}a_y \cdot {}_{AC}\zeta_y - {}_{AC}b_y \cdot {}_{BD}\zeta_y)/c_y$$

where

$${}_{AC}a_y = 1 - ({}_A k_{mz} - {}_A k_{ex})({}_C k_{mz} - {}_C k_{ex})$$
$${}_{BD}a_y = 1 - ({}_B k_{mz} - {}_B k_{ex})({}_D k_{mz} - {}_D k_{ex})$$
$${}_{AC}b_y = {}_{AC}a_y({}_C k_{mz} - {}_C k_{ey}) + ({}_C k_{mz})^2({}_A k_{mz} - {}_A k_{ex})$$
$${}_{BD}b_y = {}_{BD}a_y({}_D k_{mz} - {}_D k_{ey}) + ({}_D k_{mz})^2({}_B k_{mz} - {}_B k_{ex})$$
$$c_y = {}_{AC}a_y \cdot {}_{BD}a_y - {}_{AC}b_y \cdot {}_{BD}b_y$$
$${}_{AC}\zeta_y = {}_C k_{mz}(-{}_A\Phi^r_{ypx} + ({}_A k_{mz} - {}_A k_{ex})\,{}_C\Phi^r_{ynx}) + {}_{AC}a_y \cdot {}_C\Phi^r_{xpy}$$
$${}_{BD}\zeta_y = {}_D k_{mz}({}_B\Phi^r_{ypx} - ({}_B k_{mz} - {}_B k_{ex})\,{}_D\Phi^r_{ynx}) + {}_{BD}a_y \cdot {}_D\Phi^r_{xny}$$

and Φ^r is used to represent an intermediate quantity calculated in the same way as a standard voltage pulse, but without the undetermined internal voltage pulse. For example:

$${}_A\Phi^r_{ypx} = {}_A V'_x + Z_0 \cdot {}_A I'_z - {}_A V^i_{ynx}$$

where

$${}_A V'_x = {}_A k_{ex}({}_A V^i_{ynx} + {}_A V^i_{znx} + {}_A V^i_{zpx} + {}_A \hat{Y}^s_x \cdot {}_A V^i_{ex})$$
$${}_A I'_z = {}_A k_{mz}({}_A V^i_{xpy} - {}_A V^i_{xny} + {}_A V^i_{ynx} - {}_A V^i_{mz})$$

For the z polarization:

$${}_C V^i_{xpz} = ({}_{AC}a_z \cdot {}_{BD}\zeta_z - {}_{BD}b_z \cdot {}_{AC}\zeta_z)/c_z$$
$${}_D V^i_{xnz} = ({}_{BD}a_z \cdot {}_{AC}\zeta_z - {}_{AC}b_z \cdot {}_{BD}\zeta_z)/c_z$$

where

$${}_{AC}a_z = 1 - ({}_A k_{mx} - {}_A k_{ez})({}_C k_{mx} - {}_C k_{ez})$$
$${}_{BD}a_z = 1 - ({}_B k_{mx} - {}_B k_{ez})({}_D k_{mx} - {}_D k_{ez})$$
$${}_{AC}b_z = {}_{AC}a_z({}_C k_{my} - {}_C k_{ez}) + ({}_C k_{ez})^2({}_A k_{mx} - {}_A k_{ez})$$
$${}_{BD}b_z = {}_{BD}a_z({}_D k_{my} - {}_D k_{ez}) + ({}_D k_{ez})^2({}_B k_{mx} - {}_B k_{ez})$$
$$c_z = {}_{AC}a_z \cdot {}_{BD}a_z - {}_{AC}b_z \cdot {}_{BD}b_z$$
$${}_{AC}\zeta_z = {}_C k_{ez}({}_A\Phi^r_{ypz} - ({}_A k_{mx} - {}_A k_{ez})\,{}_C\Phi^r_{ynz}) + {}_{AC}a_z \cdot {}_C\Phi^r_{xpz}$$
$${}_{BD}\zeta_z = {}_D k_{ez}({}_B\Phi^r_{ypz} - ({}_B k_{mx} - {}_B k_{ez})\,{}_D\Phi^r_{ynz}) + {}_{BD}a_z \cdot {}_D\Phi^r_{xnz}$$

Once these four pulses are known, the other internal pulses can be calculated as for two separate pairs of nodes. For the pair AC, these pulses are:

$${}_A V^i_{ypx} = ({}_C\Phi^r_{ynx} - ({}_C k_{mz} - {}_C k_{ex})\,{}_A\Phi^r_{ypx})/{}_{AC}a_y$$
$${}_C V^i_{ynx} = ({}_A\Phi^r_{ypx} - ({}_A k_{mz} - {}_A k_{ex})\,{}_C\Phi^r_{ynx})/{}_{AC}a_y$$
$${}_A V^i_{ypz} = ({}_C\Phi^r_{ynz} - ({}_C k_{mx} - {}_C k_{ez})\,{}_A\Phi^r_{ypz})/{}_{AC}a_z$$
$${}_C V^i_{ynz} = ({}_A\Phi^r_{ypz} - ({}_A k_{mx} - {}_A k_{ez})\,{}_C\Phi^r_{ynz})/{}_{AC}a_z$$

Each of the 4 internal pulses between nodes C and D depends upon 32 external and stub pulses (7 each from nodes A and B, and 9 each from nodes C and D). If these pulses are then treated as external pulses on the node pairs AC and BD, then each of the 8 remaining internal pulses depend upon 14 external and stub pulses (7 from each node in the pair). The exact number of arithmetic operations required for the complete procedure will depend upon whether certain coefficients are stored or re-calculated at each timestep and will typically be: 120–148 additions/subtractions, 64–62 multiplications and 0–12 divisions. This compares to 24 additions/subtractions and 6 multiplications for the standard 12-port SCN [8] and to 54 additions/subtractions and 12 multiplications for the stub-loaded node (with 6 coefficients stored) [7].

For more complicated situations, for example, a corner on an infinitesimally thin plane, more nodes are connected together and it is then debatable whether it is worth simplifying the scattering procedure since this geometry occurs less frequently. In this case, the equations can be solved using a standard symbolic computation package. If the

resulting expressions cannot be easily simplified by the package, the stub values can be included to give a set of purely numeric coefficients.

SELECTION OF STUB VALUES

The stub values needed to correctly model an infinitesimally thin septum have been obtained from a systematic optimization for the structure shown in Fig. 1. For a two-dimensional system, $a = 2b$, and cubic nodes with a node spacing of $\Delta l = a/16$, the frequency of the first resonance (electric field in the plane) is correctly predicted with open-circuit stubs of normalized capacitance (relative to the capacitance of a standard node) $\hat{C}_x^s = 0.54$ and $\hat{C}_y^s = 0.54$. The second and subsequent resonances are in good agreement if an inductive stub is added $\hat{L}_z^s = 0.62$. For a cavity with the same cross-section, additional stubs must be added for the cavity resonances to be predicted accurately: $\hat{L}_x^s = 0.13$ and $\hat{L}_y^s = 0.13$. These stub values are found to give good results over a range of discretizations and also for a finned waveguide [6]. To a first approximation, they can be considered to depend on the geometry of the edge only and do not need to be re-calculated for each new system.

APPLICATION TO AN E-PLANE FILTER

The correction has been applied to the narrow band E–plane filter shown in Fig. 3. This filter has a 1% bandwidth and is particularly sensitive to coarseness error. Details of the model are described in the next paragraph. These parameters were selected to give sufficiently good results to test the coarseness error correction and were not optimized to minimize computer resources.

To model the exact dimensions, the shapes of the nodes were distorted slightly and the hybrid SCN [9] was used for the resultant non-cubic nodes. Simple matched boundary conditions were used to terminate the problem on the ends of the waveguide, at a distance of 36mm from the filter. The wave reflection coefficient was selected to minimize reflections at the center frequency of the filter. Such a simple boundary description is only appropriate for narrow band devices. An impulse excitation, of constant amplitude across the waveguide cross-section, was used to introduce energy into the system. The simulation was run for 24ns. The outputs were taken at a distance of 18mm from the filter and a single-sided linear window function was applied to the last 10% of the time-domain output to reduce truncation errors in the Fourier transform.

Typical results for zero thickness septa are shown in Fig. 4. The resolution around the septa for the first two curves is $a/32$ and $a/64$. Even with a doubling of mesh resolution (requiring 4 times the storage and 8 times the run-time) the centre frequency is still too low. The problem could be solved with a graded or multiple grid mesh, but the region of high resolution must extend significantly beyond the edges of the septa for accurate results to be obtained and the resources are still excessive.

For comparison, a curve for the same filter but with 1 mil. thick septa is shown in Fig. 5 [10], as well as the same curve shifted for zero thickness [11]. There is good agreement with the curve obtained from the corrected coarse mesh. The new method provides an order of magnitude improvement and requires essentially the same resources as the standard coarse mesh. If required, the stub values can be tuned slightly to fit the expected response even closer, but this can only be done if this is known in advance.

CONCLUSIONS

The use of a coarseness error correction allows a relatively coarse mesh to be used to model a system with negligible impact on accuracy. With the proposed method, good results have been obtained for an E-plane filter and preliminary results for more general 3-dimensional geometries have been encouraging. A reduction in the reliance on mesh refinement techniques will enable the accurate modeling of complex systems to become feasible on modest workstations.

REFERENCES

1. P. B. Johns, "A symmetrical condensed node for the TLM method", *IEEE Trans. MTT*, vol. 35, no. 4, pp 370–377, Apr 1987.
2. D. A. Al-Mukhtar and J. E. Sitch, "Transmission-line matrix method with irregularly graded space", *IEE Proc. H*, vol. 128, no. 6, pp 299–305, Dec 1981.
3. J. L. Herring and C. Christopoulos, "Solving electromagnetic field problems using a multiple grid transmission-line modeling method", *IEEE Trans. Antennas and Propagation*, scheduled for Dec 1994 issue.
4. U. Mueller, P. P. M. So and W. J. R. Hoefer, "The compensation of coarseness error in 2D TLM modelling of microwave structures", *IEEE MTT-S digest*, 1992, Paper IF1 N-2, pp 373–376.
5. A. P. Duffy, J. L. Herring, T. M. Benson and C. Christopoulos, "Improved wire modelling in TLM", *IEEE Trans. MTT*, vol. 42, no. 10, pp 1978–1983, Oct 1994.
6. J. L. Herring and W. J. R. Hoefer, "Improved correction for 3-D TLM coarseness error", *Electronics Letters*, vol. 30, no. 14, pp 1149–1150, 7 Jul 1994.
7. P. Naylor and R. Ait-Sadi, "Simple method for determining 3-D TLM nodal scattering in nonscalar problems", *Electronics Letters*, vol. 28, no. 25, pp 2253–2354, 3 Dec 1992.

8. V. Trenkic, C. Christopoulos and T. M. Benson, "New developments in the numerical simulations of RF and microwave circuits using the TLM method", *Proc. 1st Conference in Modern Satellite and Cable Systems (TELSIKS '93)*, pp 6.1–6.6, Nis, Yugoslavia, Oct 1993.
9. R. Scaramuzza and A. J. Lowery, "Hybrid symmetrical condensed node for the TLM method", *Electronics Letters*, vol. 28, no. 23, pp. 1947–1949, Nov 1990.
10. Y. C. Shih, "Design of Waveguide E-Plane Filters with All-Metal Inserts", *IEEE Trans. MTT*, vol. 32, no. 7, pp 695–704, Jul 1984.
11. Y. C. Shih and T. Itoh, "E-Plane Filters with Finite-Thickness Septa", *IEEE Trans. MTT*, vol. 31, no. 12, pp 1009–1013, Dec 1983.

ACKNOWLEDGEMENTS

This research has been funded by the Natural Sciences and Engineering Research Council of Canada, the Science Council of British Columbia, MPR Teltech Inc. of Burnaby, B.C., and the University of Victoria.

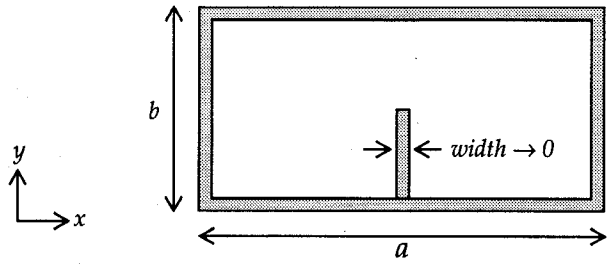

Fig. 1 Waveguide with an infinitesimally thin septum

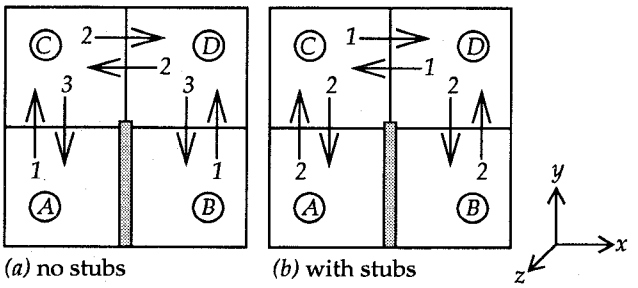

(a) no stubs (b) with stubs

Fig. 2 Transfer of voltage pulses

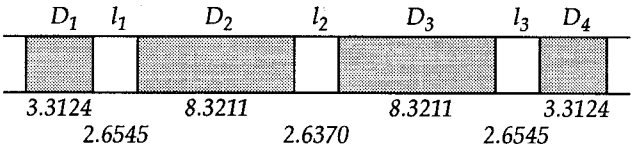

Fig. 3 E-plane filter (dimensions in mm)

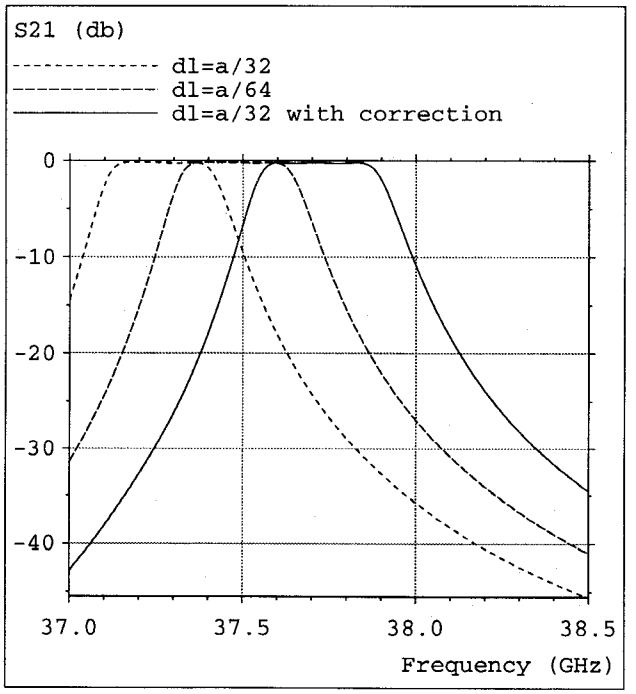

Fig. 4 S21 for the E-plane filter

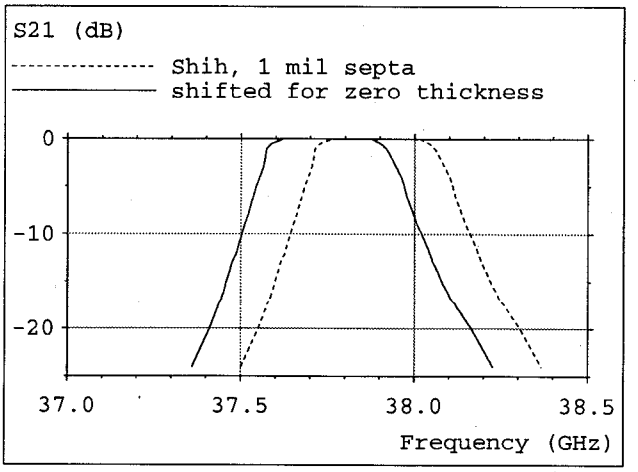

Fig. 5 Independent results for the E-plane filter